Journal of Nanobiotechnology

RESEARCH

Open Access

Leukemia-targeting NK cell nanoengagers effectively promote robust NK activation and potent anti-acute myeloid leukemia response

Hyo Jeong Kim[1*], Heejin Jun[1], Hyun Bin Lee[1], Soomin Eom[1], Junsu Kim[1], Jun Pyo Jeon[1], Sung Ho Park[1] and Sebyung Kang[1*]

Abstract

Natural killer (NK) cells are key components of innate immunity, playing a pivotal role in tumor recognition and eradication, and numerous NK cell-based immunotherapeutic approaches have been extensively investigated for cancer treatment. Here, we develop leukemia-targeting NK cell nanoengagers, termed AaLS/aCD16Nb/aCD13Nb, by simultaneously displaying NK cell-engaging nanobodies (aCD16Nb) and acute myeloid leukemia (AML)-targeting nanobodies (aCD13Nb) on lumazine synthase (AaLS) protein nanoparticles. The AaLS/aCD16Nb/aCD13Nb nanoengagers effectively bind to both NK cells and AML cells, thereby facilitating selective engagement of NK cells with leukemic targets. Through this targeted engagement, the AaLS/aCD16Nb/aCD13Nb nanoengagers promote NK cell activation, leading to enhanced interferon gamma (IFN-γ) production and robust AML cell killing in vitro. Furthermore, in AML-engraft mouse models, administration of the AaLS/aCD16Nb/aCD13Nb nanoengagers significantly reduce leukemic burden across multiple tissues, with pronounced effects in the bone marrow niche, and extend overall survival in two independent AML (U937 and THP-1) engrafted models. Collectively, our study demonstrates that this dual-ligand-displaying nanoengager platform represents a promising and potent anti-leukemic strategy, offering a multifunctional protein nanoparticles-based approach for AML immunotherapy that may be broadly adaptable to other malignancies.

Keywords Protein nanoparticle, AaLS, NK cell engager, acute myeloid leukemia

*Correspondence:
Hyo Jeong Kim
hjkim79@unist.ac.kr
Sebyung Kang
sabsab7@unist.ac.kr

Full list of author information is available at the end of the article

Graphical abstract

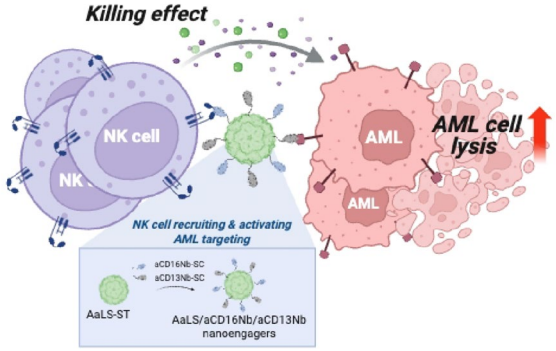

Background

Acute myeloid leukemia (AML) is an aggressive hematologic malignancy characterized by rapid proliferation and accumulation of immature myeloid cells in the bone marrow. Despite advances in AML treatment, including intensive chemotherapy, targeted agents, and allogenic hematopoietic stem cell transplantation (allo-HSCT), most patients still relapse or fail to respond, and many die from their disease [1, 2]. Outcomes are particularly poor for older patients and those with relapsed or refractory AML [3, 4].

Although immunotherapy has shown limited success in AML compared with its efficacy in solid tumors [5, 6], recent advances in chimeric antigen receptor (CAR)-T cell designs, immune checkpoint inhibition, and antibody engineering have significantly expanded the therapeutic landscape [7, 8]. Especially, recent studies highlight the pivotal role of innate immune cells, particularly natural killer (NK) cells, in effective cancer immunotherapy. NK cell-based therapeutic strategies are emerging as a safe and promising therapeutic option for AML due to their low risk of graft versus host disease (GVHD) and minimal severe side effects [9].

NK cells are cytotoxic lymphocytes essential for tumor immunosurveillance, exerting direct cytotoxicity through the release of cytotoxic granules, such as granzymes and perforin, as well as the production of inflammatory cytokines that modulate adaptive immune responses [10–12]. NK cells recognize broadly stressed cancer cells and eliminates them through regulation of the balance between activating and inhibitory receptors on their surface [11]. Given their potent anti-tumor properties, NK cell-based immunotherapies have shown promising efficacy and safety in early clinical trials [13, 14]. Recent technological advances have further enhanced their therapeutic potential by improving target cancer cell recognition and cytotoxic function [13, 15]. Thus, various NK cell -based strategies, such as NK cell engagers and CAR-NK, have been developed to potentiate NK cell-mediated cytotoxicity [12, 16].

NK cell engagers, consisting of bispecific or trispecific molecules that bridge NK cell activating receptors with tumor-associated antigens, have been demonstrated to enhance NK cell survival, proliferation, and effector functions against cancer [17, 18]. Notably, the activating receptor CD16, a high-affinity Fc receptor expressed on NK cells, efficiently triggers cytotoxicity and cytokine release, mediates antibody-dependent cellular cytotoxicity (ADCC) [19, 20], and has been extensively exploited in diverse formats of NK cell-engaging receptor designs [21–24]. However, in AML, NK cell efficacy is limited by the immunosuppressive bone marrow microenvironment, immune evasion mechanisms including downregulation of activating ligands, antigen heterogeneity, and limited in vivo persistence of NK cells [25].

Several myeloid markers, including CD33 [26–28] and CD123 [29–32], have been explored as therapeutic targets, particularly in CAR-T cell therapy and engager platforms, yet their heterogenous expression and associated toxicities remain major challenges. CD13, another antigen frequently expressed in AML, has also been investigated, as CD13-targeting protein nanoparticle displaying TRAIL molecules were shown to induce apoptosis and prolonged survival in mouse models [33].

NK cell engagers still require design strategies that promote multivalent receptor clustering, enhanced stability, and spatially defined ligand presentation, all of which are critical for maximizing NK cell activation. In this context, multivalent ligand presentation on nanoparticle scaffolds not only enables robust NK cell activation [24, 34], but also confers enhanced stability, prolonged systemic circulation, and reduced off-target interactions, making it a promising strategy to improve the efficacy of NK cell engagers. Among the various nanoparticle platforms, AaLS, a lumazine synthase protein nanoparticle derived from *Aquifex aeolicus*, self-assembles from 60 identical subunits to form a hollow icosahedral structure

[35]. Moreover, AaLS is a highly biocompatible, exceptionally thermostable and biostable protein nanoparticle with structural plasticity that enables functionalization with multiple targeting ligands and/or effector molecules through the SpyCatcher/SpyTag (SC/ST) protein ligation system [24, 33, 36–40], which enables the modular display of ligands that engage NK cell receptors while simultaneously targeting cancer-associated antigens, thereby facilitating precise cancer targeting and effective NK cell engagement.

In this study, we developed leukemia-targeting NK cell nanoengagers by applying ST-fused AaLS protein nanoparticle scaffolds simultaneously loaded with SC-fused anti-CD16 nanobody (aCD16Nb) and SC-fused anti-CD13 nanobody (aCD13Nb) (Fig. 1). The resulting construct, termed AaLS/aCD16Nb/aCD13Nb nanoengagers, was designed to physically tether NK cells to target AML cells, thereby enabling selective NK cell activation against malignant AML cells (Fig. 1). To characterize this platform, we evaluated the specificity of aCD16Nb and aCD13Nb toward NK cells and AML cells, respectively, using flow cytometry. We further evaluated the ability of the AaLS/aCD16Nb/aCD13Nb nanoengagers to mediate NK-AML cell engagement, to induce NK cell activation, and to trigger NK cell-mediated cytotoxic function in vitro, as assessed by intracellular interferon gamma (IFN-γ) detection and viability assays. Furthermore, to investigate therapeutic potential in vivo, we established AML-engrafted mouse models enabling real-time monitoring of AML progression and assessed the therapeutic efficacy of NK cells activated by the AaLS/aCD16Nb/aCD13Nb nanoengagers, including tissue-specific AML clearance. Thus, the AaLS protein nanoparticle-based NK cell nanoengagers, functionalized with cancer-targeting ligands, represents a promising platform for AML immunotherapy by harnessing NK cell effector functions to achieve selective and potent anti-leukemic activity.

Materials and methods

Cloning, protein expression and purification

A SpyTag-fused *Aquifex aeolicus* lumazine synthase subunit (AaLS-ST) gene, harboring an R108C point mutation [36], was previously constructed in a pET-Duet vector and used in this study without modification. The CD16-binding nanobody (C21 clone) [41], and the CD13-binding nanobody (Nb157 clone) [42] were genetically fused to the N-terminal end of SpyCatcher (SC) gene and cloned into the pET30b vector containing the pelB signal sequence, generating the aCD16Nb-SC and aCD13Nb-SC constructs. Plasmids encoding AaLS-ST were transformed into ClearColi™ BL21 (DE3), whereas those encoding aCD16Nb-SC or aCD13Nb-SC were transformed into competent *E. coli* strain BL21 (DE3). AaLS-ST was overexpressed at 30 ℃, and aCD16Nb-SC and aCD13Nb-SC were overexpressed at 18 ℃, all induced overnight with 0.5 mM of isopropyl β-D-1-thiogalactopyranoside (IPTG). The recombinant proteins were extracted by lysing the cells with 10 mg/ml of lysozyme, followed by sonication. AaLS-ST was

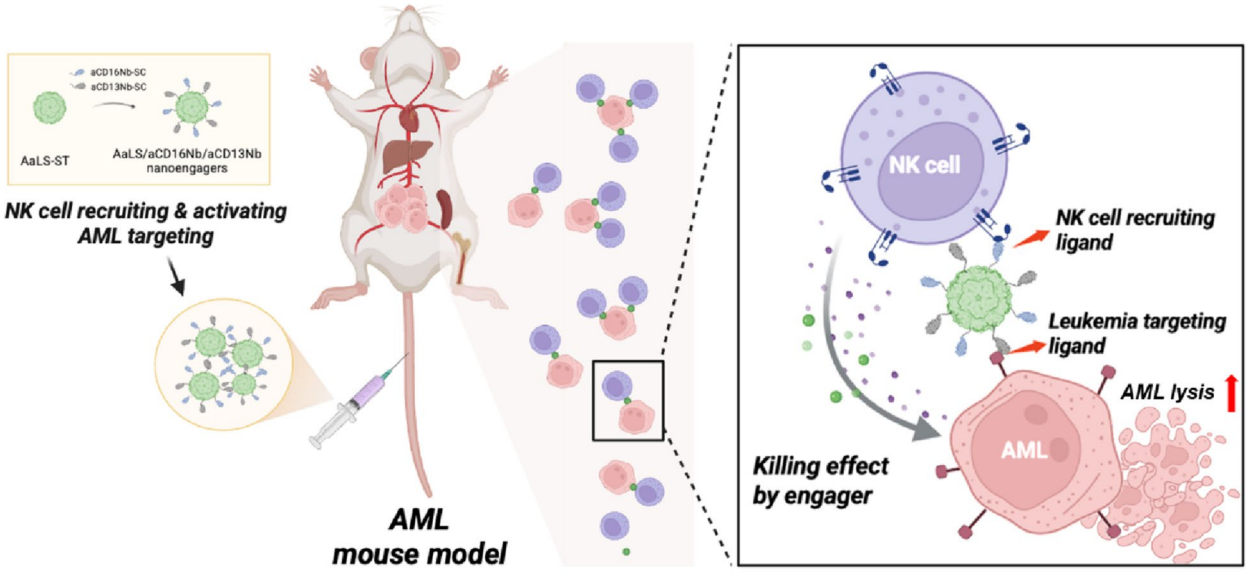

Fig. 1 Schematic illustration of the design and mechanism of action of leukemia-targeting NK cell nanoengagers. NK cell nanoengagers are designed to simultaneously display NK cell-recruiting and activating nanobodies against CD16 (aCD16Nb) and leukemia-targeting nanobodies against CD13 (aCD-13Nb) on the surface of AaLS protein nanoparticles. The AaLS/aCD16Nb/aCD13Nb nanoengagers selectvely bind NK cell and CD13-expressing acute myeloid leukemia cells, thereby promoting NK-AML cell engagement. This engagment enhances NK cell activation, resulting in potent and selective NK cell-mediated cytotoxicity against AML cells. The figure was created with BioRender.com

subjected to additional heat precipitation for 20 min at 65 ℃ to remove residual proteins prior to chromatography, as previously described [36]. The soluble protein extract was collected by centrifugation, purified using batch-type open columns (Bio-Rad) packed with a Ni Sepharose 6 Fast Flow resin (Cytiva), eluted with an elution buffer (20 mM Na_2HPO_4, 500 mM NaCl, 1 M imidazole, pH 7.4) on an NGC chromatography system (Bio-Rad), and analyzed by SDS-PAGE to determine purity and apparent molecular weight. The fractions were dialyzed against phosphate-buffered saline (PBS), and the proteins were further purified to remove endotoxins using Bio-Beads SM-2 adsorbent media (Bio-Rad). To generate single- or dual-ligand-displaying protein nanoparticles, 60-subunit AaLS-ST was incubated with nanobodies with a subunit molar ratio of 2:1 (for either aCD16Nb-SC or aCD13Nb-SC) or 2:1:1 (for both nanobodies) at 4 ℃ overnight, producing AaLS/aCD16Nb, AaLS/aCD13Nb, or AaLS/aCD16Nb/aCD13Nb, which were subsequently analyzed by size exclusion chromatography (SEC). Hydrodynamic diameters and zeta potentials of AaLS variants (AaLS-ST, AaLS/aCD16Nb, AaLS/aCD13Nb, and AaLS/aCD16Nb/aCD13Nb) were measured at 25 ℃ using dynamic light scattering (DLS; Zetasizer, Malvern). The AaLS variants were loaded into disposable polystyrene cuvettes, and the data were analyzed with Zetasizer software (Malvern Panalytical) to calculate particle sizes and standard deviations.

Preparation of human NK cells

The peripheral blood collected from healthy donors was provided by the Korean Red Cross Blood Services (Ulsan, Korea) with the approval of the Institutional Review Board (IRB) of Ulsan National Institute of Science and Technology (UNIST) (UNISTIRB-22-65-C). Human peripheral blood mononuclear cells (PBMCs) were isolated by density gradient centrifugation using Lymphoprep (STEMCELL), followed by the isolation of human NK cells from PBMCs via magnetic selection with the human NK cell isolation kit (Miltenyi Biotec), according to the manufacturer's instructions. The prepared human NK cells were either used immediately or cultured overnight in RPMI-1640 medium supplemented with 10% fetal bovine serum (FBS) (Gibco), L-glutamine (Thermo Fisher Scientific), and 1% penicillin/streptomycin (Gibco) in the presence of human IL-2 (20 ng/ml; Peprotech) at 37 °C in a humidified 5% CO_2 incubator.

Cell lines and cultures

U937, THP-1, and CCRF-CEM cell line were maintained in RPMI-1640 medium supplemented with 10% fetal bovine serum (FBS) (Gibco) and 1% antibiotic-antimycotic (Gibco). HL-60 and MV4-11 cell line were maintained in Iscove's modified Dulbecco's medium (IMDM), supplemented with 20% and 10% FBS, respectively, and 1% penicillin/streptomycin. MOLM-14 cell line was cultured in RPMI-1640 medium supplemented with 20% FBS and 1% penicillin/streptomycin. All cell lines were incubated at 37 °C in a humidified 5% CO_2 incubator. The stable luciferase-expression U937 (U937-Luc) and THP-1 (THP-1-Luc) cells were generated by transducing the cells with a lentiviral vector encoding firefly luciferase and EGFP (pLentipuro3/TO/V5-GW/EGFP-Firefly Luciferase; plasmid #119816, Addgene) and selected with puromycin (0.5 μg/mL) and cultured in RPMI-1640 medium supplemented with 10% fetal bovine serum (FBS) (Gibco) and 1% antibiotic-antimycotic (Gibco). A previously established CD13-knockout U937 cells (CD13-KO U937) was maintained as previosuly described [33].

In vitro flow cytometry

The purity of primary human NK cells isolated from PBMCs was examined by flow cytometry. Cells were stained with the Zombie Aqua™ Fixable Viability Kit (BioLegend) for 30 min, followed by Fc receptor (FcR) blocking using Human TruStain FcX™ (BioLegend) for 20 min. Cells were stained with CD56-PE/cy7 (BD Biosciences), CD3-APC (BD Biosciences), CD13-PE (BD Biosciences), and CD16-BV650 (BD Biosciences) antibodies. For detection of unconjugated anti-CD13 antibody (Invitrogen), an Alexa Fluor™ 488-conjugated anti-mouse IgG secondary antibody (ThermoFisher) was used. To evaluate the binding capability of each AaLS variant, primary human NK cells isolated from PBMCs, U937, THP-1, HL-60, and CCRF-CEM cells were incubated with 2 μM of each F5M-labeled AaLS variant (fAaLS-ST, fAaLS/aCD16Nb, fAaLS/aCD13Nb, and fAaLS/aCD16Nb/aCD13Nb) in PBS containing 3% bovine serum albumin (BSA) for 30 min. The cysteine residue at position 108 of AaLS-ST subunit was labeled with fluorescein-5-maleimide (F5M, Thermo Fisher Scientific) [43, 44] via a thiol-maleimide coupling reaction [45], and the F5M-conjugated AaLS-ST was designated fAaLS-ST. Unconjugated free F5M was removed by extensive dialysis against PBS overnight. fAaLS-ST was ligated with either CD16Nb-SC, CD13Nb-SC, or both at 4 °C overnight, generating fAaLS/aCD16Nb, fAaLS/aCD13Nb, or fAaLS/aCD16Nb/aCD13Nb. To assess the engagement of NK cells with AML cells, NK and AML cells were labeled with CellTrace™ Far-Red dye (CTFR) and CellTrace™ CFSE, respectively, according to the manufacturer's instructions (Thermo Fisher Scientific). CFSE-labeled U937 or THP-1 cells were co-cultured with CTFR-labeled NK cells in PBS containing 3% BSA and 2 μM of each AaLS variant for 1 h at 37 °C. To evaluate NK cell activation, intracellular levels of IFN-γ were measured under two experimental conditions. First, to assess the direct effect of each AaLS variant on NK cells, primary human NK cells were

seeded in 24-well plates and incubated with 2 μM of each AaLS variant for 6 h, and intracellular IFN-γ levels were measured in NK cells cultured alone. Second, to assess the activation of NK cells during co-culture with AML cells, U937, THP-1, HL-60, and CCRF-CEM cells were pre-incubated with 2 μM of each AaLS variant for 30 min at 37 °C, washed twice with PBS, and subsequently co-cultured with primary human NK cells isolated from PBMCs. For both conditions, Golgi-Plug (1 μg/ml) was added after 2 h of incubation, and cells were harvested at 6 h. Viability staining and Fc receptor blocking were performed as described above, followed by surface staining with CD56-PE/cy7 (BD Biosciences) and CD3-APC (BD Biosciences) to distinguish NK cells ($CD56^+CD3^-$) from AML cells. After washing, cells were fixed, permeabilized, and stained for intracellular IFN-γ using IFN-γ-APC/cy7 antibody (BioLegend) and the BD Cytofix/Cytoperm™ plus Fixation/Permeabilization kit (BD Biosciences) according to the manufacturer's protocol.

Cells were analyzed by flow cytometry on a BD LSR Fortessa cytometer. Data were processed and analyzed using FlowJo software.

Cell viability assay

The AaLS variants (AaLS-ST, AaLS/aCD16Nb, AaLS/aCD13Nb, and AaLS/aCD16Nb/aCD13Nb) were prepared at an initial concentration of 2 μM and subjected to 4-fold serial dilutions. The diluted variants were incubated with 2×10^4 U937, THP-1, HL-60, or CCRF-CEM cells in 96-well plates at 37 °C for 30 min. After incubation, unbound AaLS variants were removed by washing with PBS. Then, cells were cultured with or without 1×10^5 primary human NK cells isolated from PBMCs at 37 °C in a 5% CO_2 incubator for 48 h. The viability of U937, THP-1, HL-60, and CCRF-CEM cells was evaluated using the Cell Counting Kit-8 (CCK-8) assay (Dojindo). CCK-8 reagent-mixed medium was added to each well, and after 6 h of incubation, the absorbance was measured at 450 nm using a spectrophotometer (SpectraMax 190; Molecular Devices). Specific lysis (%) = (OD(Experimental)-OD(Spontaneous)/OD(Maximum)-OD (Spontaneous)) x 100%. To distinguish live and dead cells between NK and target cancer cells, the target cancer cells (U937, THP-1, HL-60, and CCRF-CEM cells) were labeled with CTFR. The labeled target cancer cells were treated with 2 μM AaLS variants at 37 °C for 30 min, washed with PBS, and then co-cultured with primary human NK cells at 37 °C for 6 h. The proportions of live and dead target cancer cells were evaluated using the LIVE/DEAD® Viability/Cytotoxicity Assay Kit (Thermo Fisher Scientific). Live cells and dead cells were stained with 0.1 μM Calcein-AM and 4 μM ethidium homodimer (EthD-1), respectively. After incubation for 15 min at room temperature, cells were analyzed by flow cytometry using a BD LSR Fortessa cytometer. Data were processed and analyzed using FlowJo software.

In vivo experiments

6–10 weeks old male in-house bred NOD.Cg-Prkdc^{scid}Il-2rg^{tm1wjl}/SzJ (NSG) (The Jackson Laboratory) mice were housed in cages of up to 5 male mice under pathogen-free conditions. All animal studies and procedures were approved by the guidance of the Institutional Animal Care and Use Committee of the Ulsan National Institute of Science and Technology (UNISTIACUC-24-67). For the first U937-Luc study, NSG mice were intravenously injected with 1×10^6 U937-Luc cells. On day 3, mice engrafted U937-Luc cells received intravenous injection of 1×10^7 PBMCs together with AaLS variants (0.1 mg/ml in 100 μl PBS) three times at 6-day intervals. On separate days, AaLS variants alone were administered (0.1 mg/ml in 100 μl PBS) twice at 6-day intervals. For the THP-1-Luc study, 5×10^6 THP-1-Luc cells were initially injected intravenously into NSG mice. 14 days later, mice received intravenous injections of 1×10^7 PBMCs along with AaLS variants (0.1 mg/ml in 100 μl PBS). After 3 days, the mice received AaLS variants alone (0.1 mg/ml in 100 μl PBS). This cycle was repeated once a week for a total of five times. The progression of the AML in each mouse was monitored every 2–3 days for 19 days in the U937-Luc model and every 3–7 days for 50 days in the THP-1-Luc model by detecting the in vivo bioluminescence imaging (BLI) signals and obtaining BLI images, following intraperitoneal injection of D-luciferin potassium salt (15 mg/ml in 200 μl PBS) as the substrate. After 15 min, the BLI images were acquired using the Bruker In Vivo Xtreme Imaging System. Survival of mice was monitored daily, and body weight was measured twice per week.

In vivo flow cytometry

In in vivo experiments assessing AML cells distribution across each tissue in the U937 model, 1×10^7 PBMCs and AaLS variants (0.1 mg/ml in 100 μl PBS) were injected intravenously into the mice 3 days after 1×10^6 U937-Luc cell injection, and the treatment was repeated three times at 3-day intervals. AML progression was monitored by in vivo BLI imaging. Four days later, mice were sacrificed, and peripheral blood, spleen, bone marrow, and liver tissue were collected and processed for flow cytometry. Peripheral blood was obtained via cardiac puncture under isoflurane anesthesia and immediately treated with Ammonium-Chloride-Potassium (ACK) lysis buffer to remove red blood cells. The spleen was mechanically dissociated using a syringe plunger, passed through a 70 μm filter, and subsequently treated with ACK lysis buffer. Bone marrow cells were obtained from the femur and tibia, passed through a 70 μm filter, and treated with ACK lysis buffer. Liver was digested in 5% RPMI

containing collagenase D for 30 min at 37 °C, then passed through a 70 μm filter. The resulting cell suspension was layered onto a Lymhoprep solution to separate immune cells from hepatocytes. Immune cells of peripheral blood, spleen, bone marrow, and liver were subjected to viability staining and Fc receptor blocking as described above, followed by staining with anti-mouse CD45-BV421 (BioLegend), anti-human CD45-APC (BioLegend), and anti-human CD13-PE (BD Biosciences). The stained cells were acquired on a BD LSR Fortessa cytometer, and the data were processed and analyzed using FlowJo software.

Fluorescence microscopy

To visualize the engagement of NK cells with AML cells, NK and AML cells were labeled with CellTrace™ Far-Red dye (CTFR) and CellTrace™ CFSE, respectively, according to the manufacturer's instructions (Thermo Fisher Scientific). CFSE-labeled U937 or THP-1 cells were co-cultured with CTFR-labeled NK cells in PBS containing 3% BSA and 2 μM of each AaLS variant for 1 h at 37 °C. The cells were fixed with 4% paraformaldehyde solution for 20 min at 4 °C and were seeded on poly-L-lysine-coated slides. Fluorescent cell images were captured using an Olympus FV1000 confocal microscopy (Olympus).

Immunoblotting

U937, THP-1, HL-60, MV4-11, MOLM-14, and CCRF-CEM cells were lysed with RIPA buffer containing halt protease inhibitor cocktail (Thermo Fisher Scientific). Proteins were resolved in SDS-polyacrylamide gel electrophoresis gel and transferred to polyvinylidene difluoride membranes. The membranes were blocked for 1 h in PBS-Tween 20 containing 5% skim milk and incubated with anti-CD13 antibody (Abcam) and β-actin (Novus Biologicals) antibody at 4 °C overnight. Membranes were washed with 0.05% PBS-T and incubated with horseradish peroxidase-conjugated secondary antibody at room temperature for 1 h. Immunoreactivity was detected using the Pierce™ ECL Western Blotting Substrate (Thermo Scientific) and chemiluminescence signal was read with a ChemiDoc Imaging Systems (Bio-Rad).

Peripheral blood analysis and immune cell profiling across major mouse organs

To evaluate the hematological toxicity and mouse immune cell profiling, A/16/13 (0.1 mg/ml in 100 μl PBS) was administered intravenously to 8-weeks-old male C57BL/6 mice every 3 days for a total of three injections. On day 10, peripheral blood was collected into EDTA-treated Microvette (Sarstedt), smeared on a slide, air-dried, fixed with 100% methanol, and stained using a Wright-Giemsa stain kit (Abcam) according to the manufacturer's instructions. Automated peripheral blood counts were obtained using a Hemavet 950 (Drew Scientific) following the manufacturer's instructions.

For mouse immune cell profiling, mice were anesthetized with isoflurane prior to peripheral blood and tissue collection. Peripheral blood was collected via cardiac puncture and immediately treated with ACK lysis buffer to remove red blood cells. Spleen was mechanically dissociated using a syringe plunger, followed by red blood cell lysis using ACK lysis buffer. Liver and lung were minced into small pieces and digested in RPMI-1640 with 5% FBS, 1 mg/ml of collagenase D (Roche) and 50 μg/ml of DNase I (Roche) at 37 ℃ with shaking at 160 rpm for 30 min. Digested tissues were filtered through a 70 μm nylon cell strainer, and hepatic immune cells were isolated using Lymphoprep (STEMCELL) density gradient centrifugation. Red blood cells in lung samples were lysed using ACK lysis buffer. Collected cells were washed, resuspended in PBS containing 2% FBS, pelleted at 1,500 rpm for 5 min, and counted. Live cells were identified using the Zombie Aqua™ Fixable Viability Kit (BioLegend), followed by Fc receptor blocking with TruStain FcXTM (BioLegend). Single cell suspensions were then stained with the following fluorophore-conjugated antibodies: anti-mouse CD45-pacific blue (BioLegend), anti-mouse CD3-PerCP/Cy5.5 (BioLegend), anti-mouse CD8-FITC (BioLegend), anti-mouse CD4-PE (BioLegend), anti-mouse Ly6G-Qdot655 (BioLegend), anti-mouse NK1.1-APC-Cy7 (BioLegend), anti-mouse CD11b-PE-Cy7 (BioLegend), anti-mouse F4/80-APC (eBioscience), anti-mouse CD11c-FITC (BD Biosciences), anti-mouse MHCII-APC (Invitrogen), and anti-mouse CD45R/B220-Alexa Fluor 594 (BioLegend). Stained samples were acquired on LSR Fortessa flow cytometer (BD Biosciences), and immune cell frequencies were analyzed using FlowJo software.

Statistics

All data were represented as mean ± SD or SEM and analyzed using GraphPad Prism 10 (GraphPad Software). Statistical differences were assessed with Mann-Whitney test, one-way analysis of variance (ANOVA), and two-way ANOVA with the Tukey's multiple comparison test.

Results and discussion

Construction and characterization of AaLS protein nanoparticles functionalized with nanobodies targeting CD16 and/or CD13

To investigate CD13 expression levels in AML and assess its potential as a therapeutic target, we first used GEPIA, a web tool that integrates data from The Cancer Genome Atlas (TCGA) and Genotype-Tissue Expression (GTEx) datasets, to compare gene expression between normal and AML samples. As shown in Fig. 2A, the data revealed that the expression of CD13 was significantly

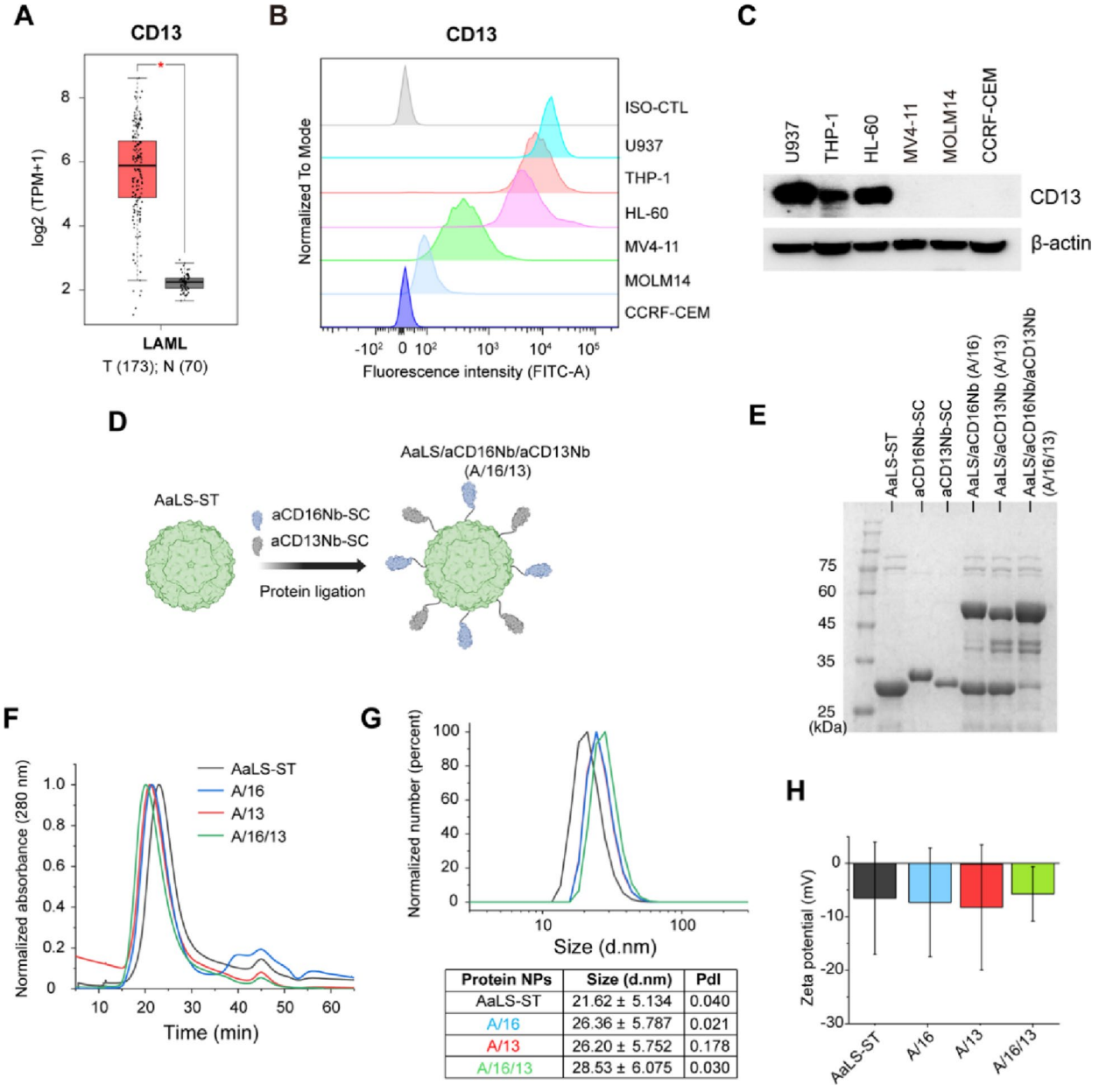

Protein NPs	Size (d.nm)	PdI
AaLS-ST	21.62 ± 5.134	0.040
A/16	26.36 ± 5.787	0.021
A/13	26.20 ± 5.752	0.178
A/16/13	28.53 ± 6.075	0.030

Fig. 2 The CD13 expression levels in AML and characterization of AaLS protein nanoparticles displaying anti-CD16 and/or anti-CD13 nanobody. (**A**) Differential expression of CD13 between AML and normal samples in the TCGA-LAML database, analyzed using the GEPIA platform. LAML: AML; T: tumor samples; N: normal samples. *$p < 0.05$. (**B** and **C**) CD13 surface expression (**B**) and protein expression (**C**) in various leukemic cell lines (U937, THP-1, MV4-11, MOLM-14, HL-60, and CCRF-CEM), analyzed by flow cytometry and immunoblotting, respectively. β-actin was used as control. (**D**) Schematic illustration of the covalent ligation of aCD16Nb-SC and aCD13Nb-SC to AaLS-ST, resulting in the formation of AaLS/aCD16Nb/aCD13Nb. (**E**) SDS-PAGE analysis of AaLS-ST, aCD16Nb-SC, aCD13Nb-SC, and the resultants following ligation: AaLS/aCD16Nb (A/16), AaLS/aCD13Nb (A/13), and AaLS/aCD16Nb/aCD13Nb (A/16/13). (**F**) SEC elution profiles of AaLS-ST, A/16, A/13, and A/16/13. (**G**) DLS analysis of AaLS-ST, A/16, A/13, and A/16/13. (**H**) Zeta potential analysis of AaLS-ST, A/16, A/13, and A/16/13

higher in patients with AML (red, $n = 173$) compared to normal samples (grey, $n = 70$). To further validate these findings, we evaluated CD13 surface expression in a panel of hematologic cancer cell lines by flow cytometry. The surface expression of CD13 was relatively high in U937, THP-1, and HL-60 cells compared to MV4-11 and MOLM-14 cells, while no detectable expression was observed in CCRF-CEM cells, a model of acute lymphoblastic leukemia (ALL) (Fig. 2B). Consistently, CD13 protein levels were also relatively high in U937, THP-1, and HL-60 cells (Fig. 2C and S1). These results suggest that CD13 expression is highly variable across hematologic cancer cell types, with both high and low expression observed in multiple cancer cell lines. Nevertheless, given

its predominant expression in many AML blasts, CD13 remains as a promising therapeutic target for AML.

To effectively harness NK cell cytotoxicity against CD13-positive AML cells, we sought to engage NK cells via CD16, a well-known activating receptor abundantly expressed on their surface, by using previously developed CD16-binding (aCD16Nb) and CD13-binding (aCD13Nb) nanobodies [24, 33] to link them to AML cells. To effectively engage activated NK cells with AML cells, we prepared previously established SpyTag (ST)-fused AaLS protein nanoparticles (AaLS-ST) [36] as nanobody-displaying nanoplatforms and SpyCatcher (SC)-fused aCD16Nb (aCD16Nb-SC) and aCD13Nb (aCD13Nb-SC) as binding ligands. These nanobodies were designed to covalently ligate to the surface of AaLS-ST via SC/ST isopeptide bonds (Fig. 2D). To generate single- or dual-ligand-displaying protein nanoparticles, 60-subunit AaLS-ST was mixed with nanobodies at a subunit molar ratio of 2:1 (for either aCD16Nb-SC or aCD13Nb-SC) or 2:1:1 (for both nanobodies). As shown in Fig. 2E, SDS-PAGE and band densitometry analysis revealed upward band shifts under single-ligand-displaying conditions, indicating that approximately 30 of the 60 AaLS-ST subunits (29.2 kDa) were covalently ligated with nanobodies, corresponding to approximately 50% occupancy (lane 4 and 5). Under dual-ligand-displaying conditions (lane 6), the appearance of an upper-shifted band and the absence of non-ligated AaLS-ST bands (29.2 kDa) indicated that both nanobodies were covalently ligated to approximately 30 subunits each, resulting in full (100%) surface coverage of the nanoparticle. Size exclusion chromatography (SEC) analysis revealed sequential elution profiles for AaLS/aCD16Nb/aCD13Nb (A/16/13), AaLS/aCD13Nb (A/13), AaLS/aCD16Nb (A/16), and AaLS-ST, in that order (Fig. 2F). Additionally, the hydrodynamic diameters of AaLS-ST and other variants were measured with dynamic light scattering (DLS). Consistent with SEC data, ligation of nanobodies resulted in an increase in particle size compared to AaLS-ST (21.62 ± 5.13 nm), with sizes of 26.20 ± 5.75 nm for AaLS/aCD13Nb, 26.36 ± 5.79 nm for AaLS/aCD16Nb, and 28.53 ± 6.08 nm for AaLS/aCD16Nb/aCD13Nb, indicating successful surface display of the ligands (Fig. 2G). Furthermore, zeta potential measurements showed that the surface charges of ligand-displayed AaLS variants were not altered (Fig. 2H), suggesting that the overall surface electrostatics remain comparable to non-ligated AaLS-ST. Taken together, these results demonstrated that ligation of aCD16Nb and/or aCD13Nb to AaLS-ST using the SC/ST system enables the formation of NK cell-engaging and leukemia-targeting nanoplatforms, while preserving the structural integrity of the protein nanoparticle.

aCD16Nb and aCD13Nb dual-ligand-displaying AaLS protein nanoparticles mediate selective engagement of NK cells to AML cells

To assess NK cell-engaging AML treatment, $CD3^-$ $CD56^+$ NK cells were first isolated from peripheral blood mononuclear cells (PBMCs) with a purity exceeding 89%, and CD16 expression on these NK cells was confirmed, as shown in Figure S2A and S2B. Next, to evaluate the specificity of nanobody-displaying AaLS variants for binding to NK and AML cells, the cells were incubated with fluorescein-5-maleimide (F5M)-labeled nanobody-displaying AaLS variants [43, 44] and then analyzed by flow cytometry. As expected, fAaLS/aCD16Nb exhibited strong and specific binding to NK cells, which are known to express high levels of CD16, while showed no binding to AML cell lines (Fig. 3A, third rows). Conversely, fAaLS/aCD13Nb showed robust binding to AML cells (U937, THP-1, and HL-60), but not to NK cells, reflecting the CD13 expression profile of these cells (Fig. 3A, fourth rows). The dual-ligand-displaying fAaLS/aCD16Nb/aCD13Nb revealed strong binding to both NK and AML cells (Fig. 3A, bottom rows), while fAaLS-ST alone showed negligible binding across all cell types (Fig. 3A, top rows). None of the fAaLS variants showed noticeable binding to CCRF-CEM cells, which lack CD13 and CD16 expression (Fig. 3A, last column). These results demonstrate that fAaLS variants displaying NK cell- and/or AML cell-binding ligands can specifically bind to their respective target cells.

To further investigate whether AaLS/aCD16Nb/aCD13Nb facilitates physical interactions between NK and AML cells, CellTrace™ CFSE-labeled U937 or THP-1 cells were co-cultured with CellTrace™ Far-Red (CTFR)-labeled NK cells in the presence of each AaLS variant. Flow cytometry analysis revealed that AaLS/aCD16Nb/aCD13Nb significantly increased the formation of double-positive populations, indicating enhanced physical engagement between NK and AML cells. Specifically, AaLS/aCD16Nb/aCD13Nb induced a markedly higher level of NK cell engagement with AML cells, showing approximately a 2-fold increase with U937 cells and an 8-fold increase with THP-1 cells relative to PBS or AaLS-ST groups (Fig. 3B). In contrast, no significant changes were observed in other groups, including PBS, AaLS-ST, AaLS/aCD16Nb, and AaLS/aCD13Nb. These results were further supported by quantitative analysis, which showed a statistically significant increase in NK-AML cell engagement in the AaLS/aCD16Nb/aCD13Nb-treated group (Fig. 3B, right panel). Importantly, this increase was consistently observed in both U937 and THP-1 cells co-cultured with NK cells, indicating a marked enhancement in NK-AML cell engagement (Fig. 3B). These results were further supported by confocal fluorescent microscopy analysis, which confirmed that AaLS/aCD16Nb/

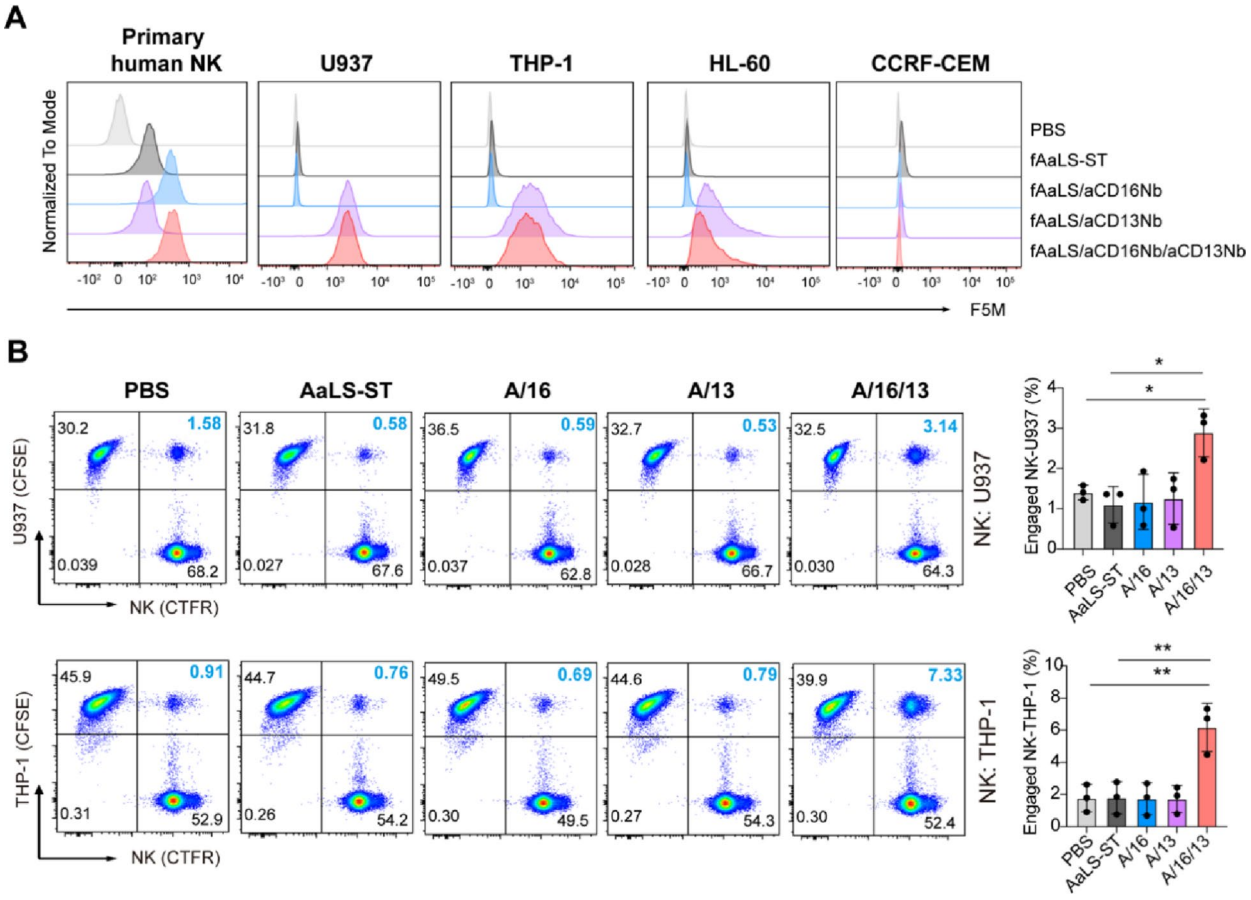

Fig. 3 Target specificity and NK-AML engagement of nanobody-displaying AaLS variants. (**A**) Binding of fluorescein-5-maleimide (F5M)-labeled each AaLS variant (fAaLS-ST, fAaLS/aCD16Nb, fAaLS/aCD13Nb, and fAaLS/aCD16Nb/aCD13Nb) to primary human NK, U937, THP1, HL-60, and CCRF-CEM cells, as analyzed by flow cytometry. (**B**) Interaction between CFSE-labeled U937 or THP-1 cells and CTFR-labeled primary human NK cells in the presence of each AaLS variant, as determined by flow cytometry. Bar graphs represent the mean ± SD from three independent experiments ($n = 3$). Statistical analysis was performed using one-way ANOVA with Tukey's multiple comparisons test. $^{*}p < 0.05$, $^{**}p < 0.01$

aCD13Nb induced close physical proximity between NK and AML cells as nanoengagers, as evidenced by co-localization and clustering of red and green signals in both U937 and THP-1 co-cultures (Figure S2C). In contrast, no significant cell-to-cell interaction was detected in PBS, AaLS-ST, AaLS/aCD16Nb, and AaLS/aCD13Nb groups, where NK and AML cells remained spatially separated (Figure S2C). Therefore, these results demonstrate that, while individual display of aCD16Nb or aCD13Nb enables specific binding to their respective cell types, simultaneous display of both on a single particle facilitates effective engagement between NK and AML cells.

The AaLS/aCD16Nb/aCD13Nb nanoengagers efficiently enhance NK cell activation

To assess the degree of NK cell activation following treatment with AaLS variants, we analyzed the levels of intracellular IFN-γ in NK cells. Primary human NK cells, isolated from PBMCs of four healthy donors, were incubated with each AaLS variant for 6 h. The aCD16Nb selectively binds to CD16 molecules on the surface of NK cells and induces NK cell activation upon binding [41]. As shown in Fig. 4A and B, flow cytometry analysis revealed that both AaLS/aCD16Nb and the AaLS/aCD16Nb/aCD13Nb nanoengagers results in increased levels of IFN-γ compared to the other groups, as observed in the previous study [24]. Notably, the AaLS/aCD16Nb/aCD13Nb nanoengagers and AaLS/aCD16Nb induced the IFN-γ levels that were approximately 77-fold and 60-fold higher, respectively, compared to PBS group, indicating effective NK cell activation upon aCD16Nb binding. In contrast, AaLS-ST and AaLS/aCD13Nb showed no detectable increase in IFN-γ production (Fig. 4A). These data indicate that the aCD16Nb displayed on AaLS variants not only facilitates specific binding to NK cells but also triggers their robust activation.

To further evaluate the degree of NK cell activation in the presence of AML cells, intracellular IFN-γ levels in NK cells were analyzed by flow cytometry following treatment with AaLS variants in co-culture with

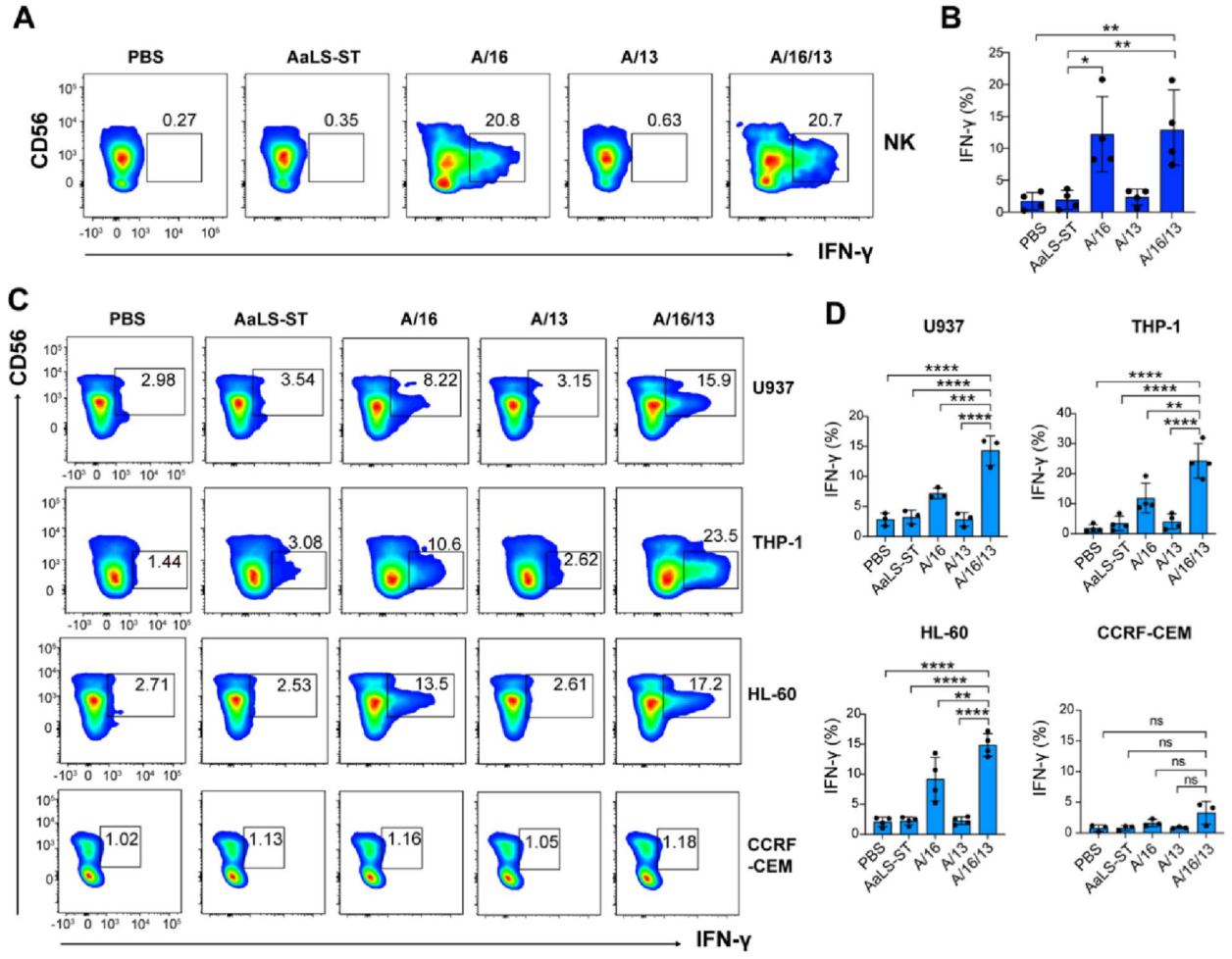

Fig. 4 NK cell activation induced by the AaLS/aCD16Nb/aCD13Nb nanoengagers. (**A** and **B**) Representative flow cytometry plots (**A**) and quantification (**B**) of intracellular IFN-γ levels in primary human NK cells ($CD56^+$ $CD3^-$) following treatment with the indicated AaLS variants for 6 h. (**C** and **D**) Representative flow cytometry plots (**C**) and quantification (**D**) of intracellular IFN-γ levels in primary human NK cells ($CD56^+$ $CD3^-$) co-cultured with U937, THP-1, HL-60, and CCRF-CEM cells pretreated with each AaLS variant for 30 min. All bar graphs represent the mean ± SD from three independent experiments ($n = 3–4$). Statistical analysis was performed using one-way ANOVA. *$p < 0.05$; **$p < 0.01$; ***$p < 0.001$; ****$p < 0.0001$; ns, not significant

AML cell lines, including U937, THP-1, and HL-60 cells. To allow sufficient and specific binding to AML cells, each AaLS variant was incubated with AML cells, followed by co-culture with NK cells. The highest levels of intracellular IFN-γ in NK cells were observed following treatment with the AaLS/aCD16Nb/aCD13Nb nanoengagers, which simultaneously bind to CD16 on NK cells and CD13 on AML cells. NK cells treated with the AaLS/aCD16Nb/aCD13Nb nanoengagers and co-cultured with U937, THP-1, HL-60 cells exhibited approximately 5-, 8- and 6-fold increases in IFN-γ production, respectively, compared to the PBS group (Fig. 4C and D). In contrast, the AaLS/aCD16Nb/aCD13Nb nanoengagers had no effect on intracellular IFN-γ levels in NK cells co-cultured with CD13-negative CCRF-CEM cells (Fig. 4C and D). These results suggest specific binding of the AaLS/aCD16Nb/aCD13Nb nanoengagers to cancer cells, followed by subsequent engagement of NK cells, is essential for triggering effective NK cell activation. Collectively, these findings indicate that the AaLS/aCD16Nb/aCD13Nb nanoengagers elicit robust NK cell activation and promote effective dual-targeting recognition through direct NK-AML cell interaction, resulting in enhanced immune responses.

NK cell activation by the AaLS/aCD16Nb/aCD13Nb nanoengagers induces potent cytotoxicity against target AML cells

To investigate whether NK cell activation induced by the AaLS/aCD16Nb/aCD13Nb nanoengagers exerts potent cytotoxicity against target AML cells, the cell viability assay was performed using the CCK-8 assay. U937, THP-1, and HL-60 cells were treated with each AaLS variant for 30 min at various concentrations and subsequently washed with PBS prior to co-culture with NK cells for 48 h. As shown in Fig. 5A, the AaLS/aCD16Nb/aCD13Nb

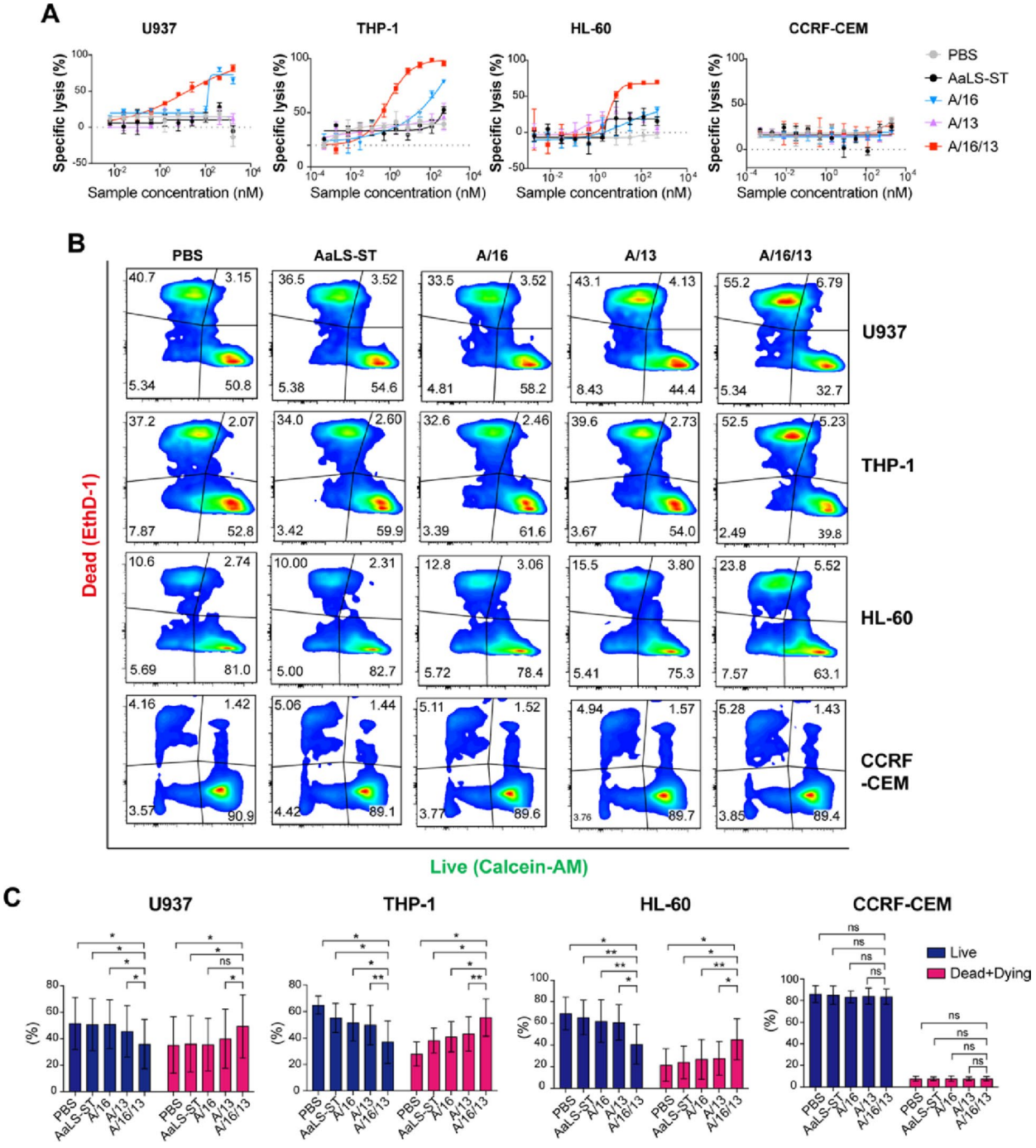

Fig. 5 Cytotoxicity of NK cells induced by the AaLS/aCD16Nb/aCD13Nb nanoengagers against various AML cell lines. (**A**) Cytotoxicity of NK cells mediated by AaLS-ST, AaLS/aCD16Nb, AaLS/aCD13Nb, and AaLS/aCD16Nb/aCD13Nb nanoengagers against AML cells, U937, THP-1, and HL-60, and CD13-negative leukemic CCRF-CEM cells. (**B**) Representative flow cytometry plots of Live/dead cell viability assay of Far-red labeled AML cells and CCRF-CEM co-cultured with NK cells in the presence of each AaLS variant. Cell viability was assessed by Calcein-AM staining for live cells (green) and EthD-1 staining for dead cells (red). (**C**) Quantification of live and dead/dying cells. Each cell line (U937, THP-1, and HL-60, $n = 5$; CCRF-CEM, $n = 3$) was co-cultured with primary human NK cells isolated from PBMCs of three to five healthy donors. Bar graphs represent the mean ± SD. Statistical analysis was performed using two-way ANOVA with Tukey's multiple comparisons test. * $P < 0.05$, ** $p < 0.01$, *** $p < 0.001$, **** $p < 0.0001$, ns, not significant

nanoengagers led to a dose-dependent increase in specific lysis of U937, THP-1, and HL-60 cells, reaching over 80% lysis at the highest concentration. These cytotoxic effects were significantly greater than those observed with AaLS-ST, AaLS/aCD16Nb, or AaLS/aCD13Nb. Notably, no cytotoxic activity was detected in CD13-negative CCRF-CEM cells (Fig. 5A), suggesting high target specificity. AaLS/aCD16Nb exhibited moderate cytotoxicity, whereas PBS or AaLS-ST alone showed minimal effects (Fig. 5A). Since both NK and AML cells are suspension cells, we further performed a flow-cytometry-based cell killing assay to overcome the limitations of the CCK-8 assay. To distinguish target AML cells from effector NK cells during co-culture, U937, THP-1, and HL-60 were first pre-labeled with CTFR, followed by incubation with each AaLS variant and subsequent co-culture with NK cells at a 5:1 effector-to-target (E: T) ratio. The NK cell-mediated cytotoxicity toward AML cells was evaluated using a live/dead assay by flow cytometry, based on Calcein-AM and EthD-1 staining, with target AML cells distinguished by gating on APC-positive fluorescence, representing CTFR-labeled cells. As shown in Figure S3A, flow cytometry plots revealed distinct changes in the proportions of Calcein-positive/EthD-1-negative (live) and EthD-1-positive (dead/dying) cell populations. The percentage of live AML cells (lower-right quadrant) among AML cells was significantly reduced in the AaLS/aCD16Nb/aCD13Nb nanoengager-treated group compared to other groups, while the proportion of dead or dying cells (upper-left and upper-right quadrants) increased markedly (Fig. 5B and C). These effects were consistent across all three AML cell lines (Fig. 5B and C). In contrast, no significant changes in proportion of live or dead/dying populations were observed in CD13-negative CCRF-CEM cells. To further validate the requirement for CD13-dependent target engagement, we performed a live/dead cell viability assay using Calcein-AM/EthD-1 staining in previously established CD13-KO U937 cells [33], which similarly showed no detectable changes in proportion of live or dead/dying populations (Figure S3B and C), indicating that direct engagement of NK cells with target AML cells, mediated by both aCD16Nb and aCD13Nb on an AaLS/aCD16Nb/aCD13Nb nanoengagers, is essential for maximal and specific NK cell-mediated killing of AML cells (Fig. 5B and C). These results were further supported by analyses using NK cells isolated from the PBMCs of multiple healthy donors, with individual results shown in Figure S4 and quantitative data presented in Fig. 5C. Across all AML cell lines, the AaLS/aCD16Nb/aCD13Nb nanoengagers significantly reduced the proportion of live cells and elevated dead/dying cell populations compared to other groups (PBS, AaLS-ST, AaLS/aCD16Nb, AaLS/aCD13Nb), with statistical significance ranging from $p < 0.05$ to $p < 0.01$ (Fig. 5). In contrast, NK cell-mediated cytotoxicity against CD13-negative CCRF-CEM cells was minimal (Fig. 5). These data indicate that a consistent pattern of NK cell-mediated enhanced cytotoxicity across donors. Collectively, NK cells engagement, effectively triggered by nanoengagers targeting CD13-positive cancer cells, leads to potent and selective NK-mediated cytotoxicity against AML cells.

The AaLS/aCD16Nb/aCD13Nb nanoengagers reduce AML burden and prolong survival in AML-engrafted NSG mice

To monitor AML burden in vivo in real time using bioluminescence imaging (BLI), stable luciferase-expressing U937 cells (U937-Luc) were generated. To evaluate anti-leukemic activity of the AaLS/aCD16Nb/aCD13Nb nanoengagers and other AaLS variants in vivo, NOD.Cg-Prkdc^{scid}Il2rg^{tm1wjl}/SzJ (NSG) mice were intravenously injected with 1×10^6 U937-Luc cells on day 0 (Fig. 6A). Since NSG mice are immunodeficient and lack functional NK cells, PBMCs engraftment was essential to reconstitute a human immune system. Given that the U937-based AML model in NSG mice is aggressive and rapidly lethal [46, 47], and that previous studies have shown that AML cells to be well established by three days post-injection [33], AaLS variants were co-administered with PBMCs once weekly and administered alone on a separate day within the same week as outlined in Fig. 6A. Mice were monitored every few days for disease progression using BLI as a readout of leukemia cell burden, according to the schedule shown in Fig. 6A. The U937-Luc-derived BLI signals was clearly detected on day 9 and reached maximal levels by day 16 (Fig. 6B). U937-Luc-engrafted mice treated with the AaLS/aCD16Nb/aCD13Nb nanoengagers exhibited a reduction in BLI signal, indicating decreased AML burden, compared to those treated with AaLS-ST, AaLS/aCD16Nb, AaLS/aCD13Nb, or PBS, all of which were co-administered with PBMCs throughout the treatment period. The most pronounced differences were observed between days 14 and 16, as shown by in vivo BLI (Fig. 6B). During disease progression, body weight of mice remained relatively stable across all treatment groups and revealed a slight decrease after approximately day 14. However, no significant differences in body weight were detected among the groups, possibly reflecting a lack of treatment-related toxicity (Fig. 6C). Indeed, the AaLS/aCD16Nb/aCD13Nb nanoengager-treated mice exhibited markedly lower BLI signal intensity, as quantified by total photon flux, compared to other groups during the later time points (days 14–19) (Fig. 6D). These data are consistent with prolonged survival and are further supported by the Kaplan-Meier survival curves (Fig. 6E). Notably, the AaLS/aCD16Nb/aCD13Nb nanoengagers led to a statistically significant

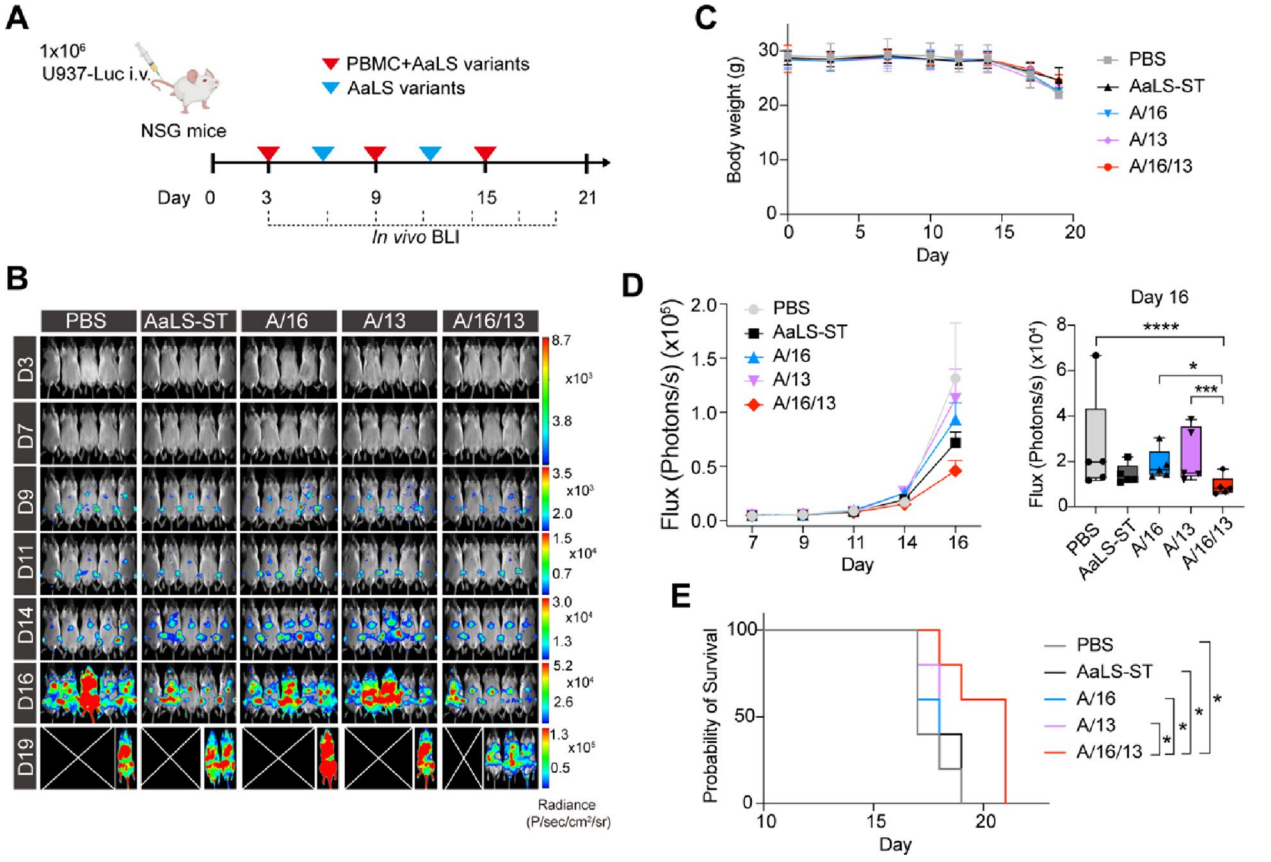

Fig. 6 In vivo efficacy of the AaLS/aCD16Nb/aCD13Nb nanoengagers in U937-engrafted NSG mice. (**A**) Experimental timeline showing intravenous (*i.v.*) injection of 1×10^6 U937-Luc cells, followed by administration of either 1×10^7 PBMCs with AaLS variant or AaLS variant alone. Bioluminescence imaging (BLI) was performed to monitor tumor progression in NSG mice ($n = 5$). (**B**) BLI signals and (**C**) body weight of U937-Luc engrafts over time in the indicated groups. (**D**) Quantification of flux (photons/s) in the experimental groups at the indicated time points. Points represent mean ± SEM. $^*p < 0.05$, $^{***}p < 0.001$; $^{****}p < 0.0001$ by mixed-effects model with Tukey's multiple comparisons test. (**E**) Kaplan-Meier survival curves of the indicated groups. $^*p < 0.05$ by log rank (Mantel-Cox) test

improvement in survival, with mortality beginning after day 16 and monitored until day 21 (Fig. 6E).

We further evaluated whether similar therapeutic benefits of the AaLS/aCD16Nb/aCD13Nb nanoengagers could be achieved in a different AML cancer model using THP-1-Luc cells (Figure S5). Compared to the U937-Luc-engrafted NSG model, THP-1-Luc cells exhibited a slower engraftment, with robust BLI signals appearing at later time points (Figure S5). Given that BLI signals indicating the onset of AML burden were detected on day 13, THP-1-Luc-engrafted mice were injected starting on day 14 with PBS, AaLS-ST, AaLS/aCD16Nb, AaLS/aCD13Nb, or AaLS/aCD16Nb/aCD13Nb nanoengagers, each co-administrated with PBMCs, as outlined in the experimental timeline (Figure S5A). At early time points (Day 13 to 19), BLI signals of low level were detected across all groups, and no significant differences in BLI signal intensity were observed. However, at mid-stage (Day 26 to 36), a marked increase in BLI signals indicated rapid leukemic progression (Figure S5B and S5D). The AaLS/aCD16Nb/aCD13Nb nanoengager-treated mice consistently showed the lowest BLI signals compared to other AaLS variants, suggesting reduced leukemic growth (Figure S5B and S5D). At later time points (Day 40 to 50), the BLI signals were strong and widespread throughout the bodies of the mice (Figure S5B). Nevertheless, the AaLS/aCD16Nb/aCD13Nb nanoengager-treated mice exhibited attenuated leukemic burden, with several mice maintaining relatively low BLI signals through day 50 compared to other AaLS variants (Figure S5B and S5D). As shown in Figure S5C, the body weight of the mice remained comparable across all treatment groups. Consistent with reduced leukemic burden analyzed by BLI, the AaLS/aCD16Nb/aCD13Nb nanoengager-treated mice demonstrated a significantly prolonged survival compared to other AaLS variants (Figure S5E). Collectively, these data indicate that engagement of NK cells targeting CD13-positive cancer cells via dual-ligand-displaying nanoengagers effectively reduces leukemic burden and extends survival in two independent AML models, supporting its therapeutic efficacy in vivo.

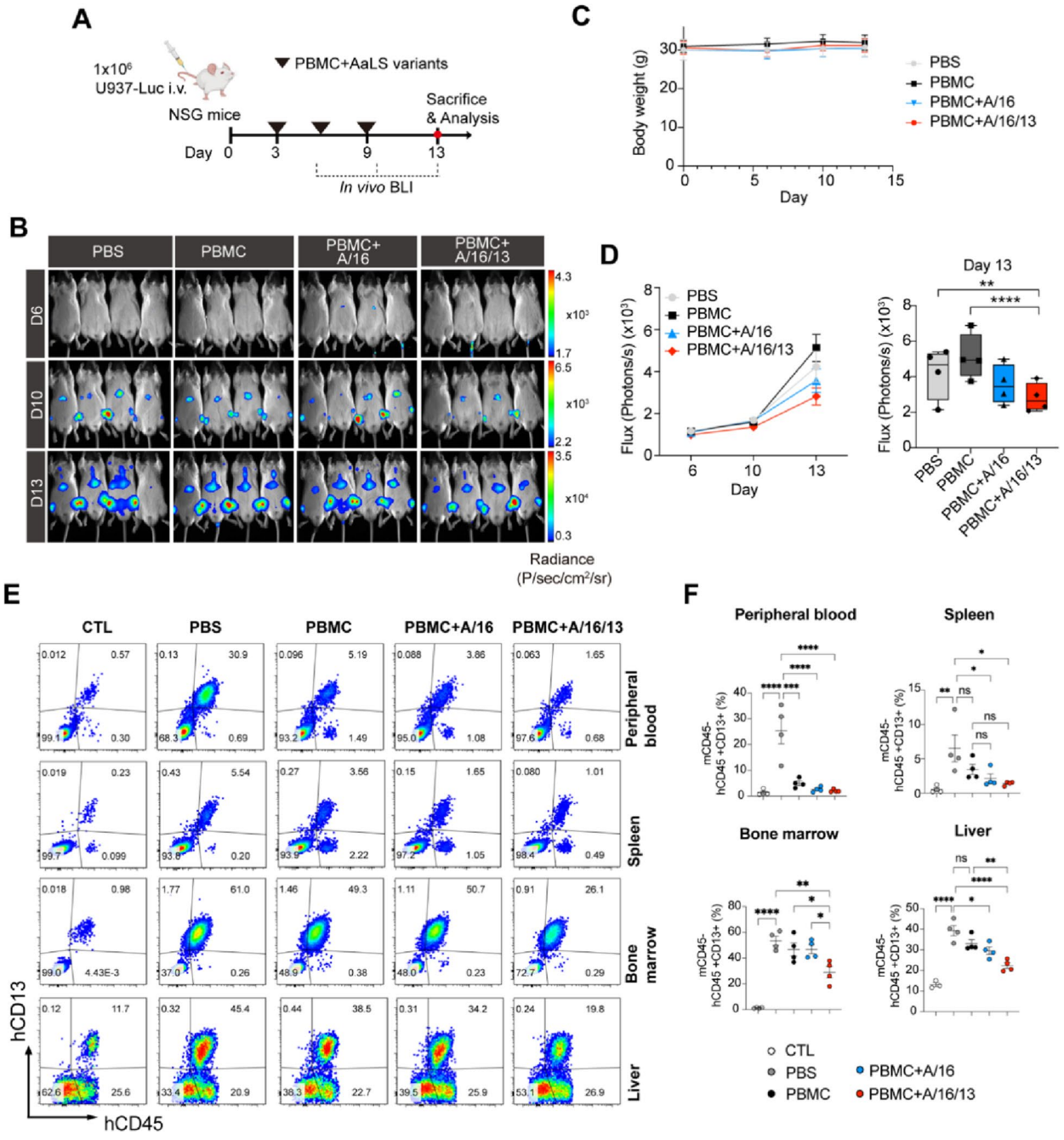

Fig. 7 The AaLS/aCD16Nb/aCD13Nb nanoengager-mediated tissue-specific clearance of AML in U937-engrafted NSG mice. (**A**) Experimental timeline showing intravenous (*i.v.*) injection of 1×10^6 U937-Luc cells, followed by administration of 1×10^7 PBMCs with AaLS variant, and bioluminescence imaging (BLI) monitoring in NSG mice ($n = 4$). (**B**) BLI signals and (**C**) body weight of U937-Luc engrafts over time in the indicated groups. (**D**) Quantification of flux (photons/s) in the experimental groups at the indicated time points. Points represent mean ± SEM. $^{**}p < 0.01$, $^{****}p < 0.0001$ by two-way ANOVA (mixed-effects model) with Tukey's multiple comparisons test. (**E**) Representative flow cytometry plots showing human $CD45^+$ $CD13^+$ frequency of cells isolated from peripheral blood, spleen, bone marrow, and liver. (**F**) Quantification of mouse $CD45^-$ human $CD45^+CD13^+$ AML cells frequency. Points represent mean ± SEM.$^*P < 0.05$, $^{**}p < 0.01$, $^{***}p < 0.001$, $^{****}p < 0.0001$ by one-way ANOVA with Tukey's multiple comparisons test. ns, not significant

In addition to BLI analyses, we performed flow cytometry analysis to monitor AML cell counts in the peripheral blood, spleen, bone marrow, and liver. The NSG mice were intravenously injected with 1×10^6 U937-Luc cells on day 0, followed by administration of PBMCs and AaLS variants on days 3, 6, and 9. The BLI was performed between days 3 and 13, and mice were sacrificed on day 13 for flow cytometry analysis (Fig. 7A). Consistent with the previously observed U937-Luc data, the AaLS/aCD16Nb/aCD13Nb nanoengager-treated mice

exhibited significantly lower BLI signal intensity on day 13 compared with PBS and PBMC groups, as confirmed by total photon flux quantification (Fig. 7B and D), with no differences in body weight among the groups (Fig. 7C). U937-Luc-engrafted mice exhibited a significant increase in human $CD45^+$ $CD13^+$ leukemic cell populations in the peripheral blood, spleen, bone marrow, and liver compared to non-engrafted control group (Fig. 7E). Human $CD45^+$ cell populations were clearly distinguishable from mouse $CD45^+$ cells, and human $CD13^+$ cells were subsequently gated within the human $CD45^+$ populations in each tissue (Figure S6). Overall, mice treated with the AaLS/aCD16Nb/aCD13Nb nanoengagers showed a significant reduction in human $CD45^+$ $CD13^+$ leukemic cells across all organs compared to the PBS group (Fig. 7F). In the peripheral blood and spleen, the AaLS/aCD16Nb/aCD13Nb nanoengager-treated mice showed frequencies of human $CD45^+$ $CD13^+$ leukemic cells comparable to those in AaLS/aCD16Nb-treated mice (Fig. 7F). In contrast, in the bone marrow, an immune-privileged organ and primary location of AML cell generation, the AaLS/aCD16Nb/aCD13Nb nanoengager-treated mice revealed the lowest frequency of human $CD45^+$ $CD13^+$ leukemic cells among PBS, PBMC alone, and PBMC with AaLS/aCD16Nb-treated group (Fig. 7F). In the liver, the AaLS/aCD16Nb/aCD13Nb nanoengager-treated mice exhibited a significantly lower frequency of human $CD45^+$ $CD13^+$ leukemic cells compared to PBS and PBMC-treated group, and a slight tendency to decrease relative to AaLS/aCD16Nb-treated group, although the difference was not statistically significant (Fig. 7E and F). In the peripheral bloodstream, both AaLS/aCD16Nb/aCD13Nb nanoengagers and AaLS/aCD16Nb treatments were most effective in elimination of circulating human $CD45^+$ $CD13^+$ leukemic cells, likely due to the relatively low number of AML cells circulating within the bloodstream compared to other tissues, as well as more frequent interactions with exogenously administered PBMCs. Additionally, the greater reduction in leukemic cells in the bone marrow following the AaLS/aCD16Nb/aCD13Nb nanoengager treatment highlights the important role of CD13 targeting within the bone marrow niche, where CD16-mediated targeting alone was insufficient. These results indicates that CD13 targeting enhanced the local accumulation of CD16-engaged NK cells within the bone marrow, thereby facilitating more frequent interaction with $CD13^+$ AML cells and improving anti-leukemic activity. Finally, to assess the potential off-target hematological toxicity and alterations in immune cell profiles associated with the AaLS protein nanoparticle serving as the scaffold for AaLS/aCD16Nb/aCD13Nb under immunocompetent conditions, peripheral blood, spleen, liver and lung tissues from mice intravenously administered with AaLS/aCD16Nb/aCD13Nb were subjected to hematological analysis and flow cytometry-based immune cell profiling. No significant changes in body weight were observed following AaLS/aCD16Nb/aCD13Nb treatment compared to controls (Figure S7A). Hematological parameters, including white blood cells (WBCs), red blood cells (RBCs), hemoglobin (Hb), hematocrit (HCT), mean corpuscular volume (MCV), and platelets (PLTs), at day 10 were comparable between AaLS/aCD16Nb/aCD13Nb- and PBS-treated mice, consistent with representative Wright-Giemsa-stained peripheral smears showing no apparent morphological abnormalities (Figure S7B and C). Furthermore, immune cell frequencies across macrophage, T cell, NK cell, neutrophil, cDC, and B cell populations in peripheral blood, spleen, liver, and lung were comparable between AaLS/aCD16Nb/aCD13Nb- and PBS-treated mice, as assessed by flow cytometry (Figure S7D-F). Thus, no overt hematological toxicity or significant alterations in immune cell populations were observed following AaLS/aCD16Nb/aCD13Nb administration, indicating a favorable safety profile of the AaLS-based nanoengager in vivo.

Collectively, these data indicate that engagement of NK cells induced by the AaLS/aCD16Nb/aCD13Nb nanoengagers mediates AML cell clearance with tissue-specific efficacy, demonstrating the therapeutic potential for targeting AML cells, especially within the bone marrow. It remains apparent that complete AML eradication was not achieved, highliting the need for further optimization. Building on evidence that IL-2 or IL-15 enhances NK cell survival, proliferation, and function [48–52], strategies such as cytokine supplementation or cytokine-combined nanoengager configurations designed to reinforce NK cell persistence may improve therapeutic efficacy and therefore warrant further investigation.

Conclusions

In this study, we established a leukemia-targeting NK cell nanoengager, AaLS/aCD16Nb/aCD13Nb, constructed from ST-fused AaLS protein nanoparticle scaffolds simultaneously displaying SC-fused anti-CD16 and anti-CD13 nanobodies. The SC/ST protein ligation system enabled efficient, simultaneous surface display of aCD16Nb and aCD13Nb on AaLS-ST, generating an NK cell-engaging and leukemia-targeting nanoengager while preserving the structural integrity of the protein nanoparticle.

The AaLS/aCD16Nb/aCD13Nb nanoengagers effectively bound to both NK and AML cells, facilitating their physical interaction and promoting specific NK-AML cell engagement. Upon AML cell engagement, the AaLS/aCD16Nb/aCD13Nb nanoengagers robustly activated NK cells and induced potent cytotoxic responses in vitro, as evidenced by elevated IFN-γ production and significant AML cell killing.

Treatment with the AaLS/aCD16Nb/aCD13Nb nanoengagers markedly reduced leukemic burden and prolonged survival in two independent AML (U937 and THP-1) engrafted models. In the U937 model, it decreased $CD45^{+}CD13^{+}$ leukemic cells across blood, spleen, bone marrow, and liver, highlighting the importance of CD13 targeting for NK cell activity within immune-privileged niches. Although complete AML eradication was not achieved, strategies to enhance NK cell persistence and overcome the immunosuppressive bone marrow microenvironment could further improve therapeutic efficacy.

Taken together, our findings suggest that the AaLS/aCD16Nb/aCD13Nb nanoengager is a versatile and target-specific NK cell engager that effectively harnesses NK cell effector functions to achieve selective anti-leukemic activity. Beyond AML, this platform offers a potent immunotherapy strategy that could be extended to other cancer types by modifying its targeting ligands, thereby providing new opportunities for the development of next-generation NK cell-based therapies.

Abbreviations

AML	Acute myeloid leukemia
NK	Natural killer
ADCC	Antibody-dependent cellular cytotoxicity
PBMCs	Peripheral blood mononuclear cells
HSCT	Hematopoietic stem cell transplantation
GVHD	Graft versus host disease
AaLS	Aquifex aeolicus lumazine synthase
CTFR	CellTrace™ Far-Red
IFN-γ	Interferon gamma
F5M	Fluorescein-5-maleimide
BLI	Bioluminescence imaging
SC	SpyCatcher
ST	SpyTag

Supplementary Information

The online version contains supplementary material available at https://doi.org/10.1186/s12951-026-04233-4.

Supplementary Material 1

Acknowledgements

We thank UNIST Office of Research Facilities and Training (ResFacT) for support of using the equipment.

Author contributions

Hyo Jeong Kim: Conceptualization, Investigation, Data Curation, Methodology, Visualization, Writing-Original Draft, Funding acquisition, Writing-Review & Editing; Heejin Jun: Investigation & Methodology; Hyun Bin Lee: Investigation & Methodology; Soomin Eom: Methodology & Visualization; Junsu Kim: Methodology & Visualization; Jun Pyo Jeon: Resources; Sung Ho Park: Resources; Sebyung Kang: Conceptualization, Investigation, Data Curation, Methodology, Visualization, Writing-Original Draft, Funding acquisition, Writing-Review, Editing & Supervision.

Funding

This work was supported by the National Research Foundation of Korea (NRF) grant (RS-2018-NR031072 and RS-2023-00245318) funded by the Korean Government.

Data availability

The data supporting this article have been included as part of the SI and the additional data that support the findings of this study are available from the corresponding author upon reasonable request.

Declarations

Ethics approval and consent to participate

All animal studies and procedures were approved by the guidance of the Institutional Animal Care and Use Committee of the Ulsan National Institute of Science and Technology (UNISTIACUC-24-67). The peripheral blood collected from healthy donors was provided by the Korean Red Cross Blood Services (Ulsan, Korea) with the approval of the Institutional Review Board (IRB) of Ulsan National Institute of Science and Technology (UNIST) (UNISTIRB-22-65-C).

Consent for publication

Not applicable.

Competing interests

The authors declare no competing interests.

Author details

[1]Department of Biological Sciences, Ulsan National Institute of Science and Technology (UNIST), Ulsan 44919, Korea

Received: 2 January 2026 / Accepted: 22 February 2026
Published online: 06 March 2026

References

1. Craddock C, Friedberg JW. Immunotherapy for Hematologic Malignancies. J Clin Oncol. 2021;39:343–5.
2. Sorror ML, Maris MB, Storb R, Baron F, Sandmaier BM, Maloney DG, et al. Hematopoietic cell transplantation (HCT)-specific comorbidity index: a new tool for risk assessment before allogeneic HCT. Blood. 2005;106:2912–9.
3. Burnett A, Wetzler M, Lowenberg B. Therapeutic advances in acute myeloid leukemia. J Clin Oncol. 2011;29:487–94.
4. Dohner H, Weisdorf DJ, Bloomfield CD. Acute Myeloid Leukemia. N Engl J Med. 2015;373:1136–52.
5. Gomez-Llobell M, Peleteiro Raindo A, Climent Medina J, Gomez Centurion I, Mosquera Orgueira A. Immune Checkpoint Inhibitors in Acute Myeloid Leukemia: A Meta-Analysis. Front Oncol. 2022;12:882531.
6. Sanmamed MF, Chen L. A Paradigm Shift in Cancer Immunotherapy: From Enhancement to Normalization. Cell. 2019;176:677.
7. Daver N, Alotaibi AS, Bucklein V, Subklewe M. T-cell-based immunotherapy of acute myeloid leukemia: current concepts and future developments. Leukemia. 2021;35:1843–63.
8. Liu Y, Wang W, Wang C, Deng J, Hu Y, Mei H, et al. Recent advances of chimeric antigen receptor T-cell therapy for acute myeloid leukemia. Front Immunol. 2025;16:1572407.
9. Zhang L, Zhao Y, Dong Y, Jiang X. NK cell-based immunotherapy strategies for myeloid leukemia. Front Immunol. 2025;16:1621885.
10. Zamai L, Ahmad M, Bennett IM, Azzoni L, Alnemri ES, Perussia B. Natural killer (NK) cell-mediated cytotoxicity: Differential use of TRAIL and Fas ligand by immature and mature primary human NK cells. J Exp Med. 1998;188:2375–80.
11. Myers JA, Miller JS. Exploring the NK cell platform for cancer immunotherapy. Nat Rev Clin Oncol. 2021;18:85–100.
12. Wolf NK, Kissiov DU, Raulet DH. Roles of natural killer cells in immunity to cancer, and applications to immunotherapy. Nat Rev Immunol. 2023;23:90–105.
13. Page A, Chuvin N, Valladeau-Guilemond J, Depil S. Development of NK cell-based cancer immunotherapies through receptor engineering. Cell Mol Immunol. 2024;21:315–31.
14. Heipertz EL, Zynda ER, Stav-Noraas TE, Hungler AD, Boucher SE, Kaur N, et al. Current Perspectives on Off-The-Shelf Allogeneic NK and CAR-NK Cell Therapies. Front Immunol. 2021;12:732135.
15. Shimasaki N, Jain A, Campana D. NK cells for cancer immunotherapy. Nat Rev Drug Discov. 2020;19:200–18.
16. Xu J, Niu T. Natural killer cell-based immunotherapy for acute myeloid leukemia. J Hematol Oncol. 2020;13:167.

17. Gauthier L, Morel A, Anceriz N, Rossi B, Blanchard-Alvarez A, Grondin G, et al. Multifunctional natural killer cell engagers targeting NKp46 trigger protective tumor immunity. Cell. 2019;177:1701–e1316.
18. Sarha D, Brandt L, Felices M, Guldevall K, Lenvik T, Hinderlie P, et al. 161533 TriKE stimulates NK-cell function to overcome myeloid-derived suppressor cells in MDS. Blood Adv. 2018;2:1459–69.
19. Bhatnagar N, Ahmad F, Hong HS, Eberhard J, Lu IN, Ballmaier M, et al. FcgammaRIII (CD16)-mediated ADCC by NK cells is regulated by monocytes and FcgammaRII (CD32). Eur J Immunol. 2014;44:3368–79.
20. Gleason MK, Verneris MR, Todhunter DA, Zhang B, McCullar V, Zhou SX, et al. Bispecific and trispecific killer cell engagers directly activate human NK cells through CD16 signaling and induce cytotoxicity and cytokine production. Mol Cancer Ther. 2012;11:2674–84.
21. Reusing SB, Vallera DA, Manser AR, Vatrin T, Bhatia S, Felices M, et al. CD16xCD33 Bispecific Killer Cell Engager (BiKE) as potential immunotherapeutic in pediatric patients with AML and biphenotypic ALL. Cancer Immunol Immunother. 2021;70:3701–8.
22. Nikkhoi SK, Li G, Eleya S, Yang G, Vandavasi VG, Hatefi A. Bispecific killer cell engager with high affinity and specificity toward CD16a on NK cells for cancer immunotherapy. Front Immunol. 2023;13:1039969.
23. Yun HD, Felices M, Vallera DA, Hinderlie P, Cooley S, Arock M, et al. Trispecific killer engager CD16xIL15xCD33 potently induces NK cell activation and cytotoxicity against neoplastic mast cells. Blood Adv. 2018;2:1580–4.
24. Park SG, Kim HJ, Lee HB, Eom S, Jun H, Jang Y, et al. Protein cage nanoparticle-based NK cell-engaging nanodrones (NKeNDs) effectively recruit NK cells to target tumor sites and suppress tumor growth. Nano Today. 2024;54:102075.
25. Carlsten M, Jaras M. Natural Killer Cells in Myeloid Malignancies: Immune Surveillance, NK Cell Dysfunction, and Pharmacological Opportunities to Bolster the Endogenous NK Cells. Front Immunol. 2019;10:2357.
26. Kenderian SS, Ruella M, Shestova O, Klichinsky M, Aikawa V, Morrissette JJ, et al. CD33-specific chimeric antigen receptor T cells exhibit potent preclinical activity against human acute myeloid leukemia. Leukemia. 2015;29:1637–47.
27. Kim MY, Yu KR, Kenderian SS, Ruella M, Chen S, Shin TH, et al. Genetic Inactivation of CD33 in Hematopoietic Stem Cells to Enable CAR T Cell Immunotherapy for Acute Myeloid Leukemia. Cell. 2018;173:1439–e5319.
28. Wang QS, Wang Y, Lv HY, Han QW, Fan H, Guo B, et al. Treatment of CD33-directed chimeric antigen receptor-modified T cells in one patient with relapsed and refractory acute myeloid leukemia. Mol Ther. 2015;23:184–91.
29. Mardiros A, Dos Santos C, McDonald T, Brown CE, Wang X, Budde LE, et al. T cells expressing CD123-specific chimeric antigen receptors exhibit specific cytolytic effector functions and antitumor effects against human acute myeloid leukemia. Blood. 2013;122:3138–48.
30. Luo Y, Chang LJ, Hu YX, Dong LJ, Wei GQ, Huang H. First-in-Man CD123-Specific Chimeric Antigen Receptor-Modified T Cells for the Treatment of Refractory Acute Myeloid Leukemia. Blood. 2015;126:3778.
31. Sugita M, Galetto R, Zong HL, Ewing-Crystal N, Trujillo-Alonso V, Mencia-Trinchant N, et al. Allogeneic TCRαβ deficient CAR T-cells targeting CD123 in acute myeloid leukemia. Nat Commun. 2022;13:2227.
32. Gauthier L, Virone-Oddos A, Beninga J, Rossi B, Nicolazzi C, Amara C, et al. Control of acute myeloid leukemia by a trifunctional NKp46-CD16a-NK cell engager targeting CD123. Nat Biotechnol. 2023;41:1296–306.
33. Jun H, Yeo M, Jeon JP, Eom S, Kim HJ, Kim Y, et al. CD13-targeting and TRAIL-displaying protein nanoparticles effectively induce apoptotic cell death of acute myeloid leukemia, prolonging survival in mouse models. Nano Today. 2024;59:102474.
34. Au KM, Park S, Wang AZ. Trispecific natural killer cell nanoengagers for targeted chemoimmunotherapy. Sci Adv. 2020;6:eaba8564.
35. Zhang X, Meining W, Fischer M, Bacher A, Ladenstein R. X-ray structure analysis and crystallographic refinement of lumazine synthase from the hyperthermophile Aquifex aeolicus at 1.6 A resolution: determinants of thermostability revealed from structural comparisons. J Mol Biol. 2001;306:1099–114.
36. Choi H, Choi B, Kim GJ, Kim HU, Kim H, Jung HS, et al. Fabrication of Nanoreaction Clusters with Dual-Functionalized Protein Cage Nanobuilding Blocks. Small. 2018;14:e1801488.
37. Zakeri B, Fierer JO, Celik E, Chittock EC, Schwarz-Linek U, Moy VT, et al. Peptide tag forming a rapid covalent bond to a protein, through engineering a bacterial adhesin. Proc Natl Acad Sci U S A. 2012;109:E690–7.
38. Choi H, Yeo M, Kang Y, Kim HJ, Park SG, Jang E, et al. Lactate oxidase/catalase-displaying nanoparticles efficiently consume lactate in the tumor microenvironment to effectively suppress tumor growth. J Nanobiotechnol. 2023;21:5.
39. Jun H, Jang E, Kim H, Yeo MR, Park SG, Lee J, et al. TRAIL & EGFR affibody dual-display on a protein nanoparticle synergistically suppresses tumor growth. J Control Release. 2022;349:367–78.
40. Eom S, Park SG, Jun H, Kim Y, Lee HB, Kang S. Effective delivery of diphtheria toxin using protein cage nanoparticles for targeted cancer therapy. Acta Biomater. 2025;202:517–28.
41. Behar G, Siberil S, Groulet A, Chames P, Pugniere M, Boix C, et al. Isolation and characterization of anti-FcgammaRIII (CD16) llama single-domain antibodies that activate natural killer cells. Protein Eng Des Sel. 2008;21:1–10.
42. He X, Feng Z, Ma J, Ling S, Cao Y, Gurung B, et al. Bispecific and split CAR T cells targeting CD13 and TIM3 eradicate acute myeloid leukemia. Blood. 2020;135:713–23.
43. Kim H, Kang YJ, Min J, Choi H, Kang S. Development of an antibody-binding modular nanoplatform for antibody-guided targeted cell imaging and delivery. RSC Adv. 2016;6:19208–13.
44. Min J, Kim S, Lee J, Kang S. Lumazine synthase protein cage nanoparticles as modular delivery platforms for targeted drug delivery. RSC Adv. 2014;4:48596–600.
45. Renault K, Fredy JW, Renard PY, Sabot C. Covalent Modification of Biomolecules through Maleimide-Based Labeling Strategies. Bioconjug Chem. 2018;29:2497–513.
46. Rennert PD, Dufort FJ, Su L, Sanford T, Birt A, Wu L, et al. Anti-CD19 CAR T Cells That Secrete a Biparatopic Anti-CLEC12A Bridging Protein Have Potent Activity Against Highly Aggressive Acute Myeloid Leukemia In Vitro and In Vivo. Mol Cancer Ther. 2021;20:2071–81.
47. Petrov JC, Wada M, Pinz KG, Yan LE, Chen KH, Shuai X, et al. Compound CAR T-cells as a double-pronged approach for treating acute myeloid leukemia. Leukemia. 2018;32:1317–26.
48. Ranson T, Vosshenrich CA, Corcuff E, Richard O, Muller W, Di Santo JP. IL-15 is an essential mediator of peripheral NK-cell homeostasis. Blood. 2003;101:4887–93.
49. Huntington ND, Puthalakath H, Gunn P, Naik E, Michalak EM, Smyth MJ, et al. Interleukin 15-mediated survival of natural killer cells is determined by interactions among Bim, Noxa and Mcl-1. Nat Immunol. 2007;8:856–63.
50. Huntington ND, Legrand N, Alves NL, Jaron B, Weijer K, Plet A, et al. IL-15 trans-presentation promotes human NK cell development and differentiation in vivo. J Exp Med. 2009;206:25–34.
51. Wiedemann GM, Grassmann S, Lau CM, Rapp M, Villarino AV, Friedrich C, et al. Divergent Role for STAT5 in the Adaptive Responses of Natural Killer Cells. Cell Rep. 2020;33:108498.
52. Fehniger TA, Bluman EM, Porter MM, Mrozek E, Cooper MA, VanDeusen JB, et al. Potential mechanisms of human natural killer cell expansion in vivo during low-dose IL-2 therapy. J Clin Invest. 2000;106:117–24.

Publisher's note